REPORT DOCUMENTATION PAGE

Form Approved
OMB No. 0704-0188

1. REPORT DATE *(DD-MM-YYYY)*
10-02-2007

REPRINT

4. TITLE AND SUBTITLE
Solar Radio Burst and Solar Wind Associations with Inferred Near-Relativistic Electron Injections

5a. CONTRACT NUMBER

5b. GRANT NUMBER

5c. PROGRAM ELEMENT NUMBER
61102F

6. AUTHOR(S)
Kahler, S.W, H. Aurass*, G. Mann*, and A. Klassen**

5d. PROJECT NUMBER
2311

5e. TASK NUMBER
RD

5f. WORK UNIT NUMBER
A1

7. PERFORMING ORGANIZATION NAME(S) AND ADDRESS(ES)
Air Force Research Laboratory/VSBXS
29 Randolph Road
Hanscom AFB MA 01731-3010

8. PERFORMING ORGANIZATION REPORT NUMBER
AFRL-VS-HA-TR-2007-1051

9. SPONSORING / MONITORING AGENCY NAME(S) AND ADDRESS(ES)

10. SPONSOR/MONITOR'S ACRONYM(S)
AFRL/VSBXS

11. SPONSOR/MONITOR'S REPORT NUMBER(S)

12. DISTRIBUTION / AVAILABILITY STATEMENT
Approved for Public Release; Distribution Unlimited.

*Asrophysikalisches Institute Potsdam, Germany
**Institut fur Experimentelle und Angewandte Physik, Univ of Kiel, Germany

13. SUPPLEMENTARY NOTES
REPRINTED FROM: The Astrophysical Journal, Vol 656, pp 567-576, Feb 10, 2007.

14. ABSTRACT

The solar injections of near-relativistic (NR) electron events observed at 1 AU appear to be systematically delayed by ~10 minutes from the associated flare impulsive phases. We compare inferred injection times of 80 electron events observed by the 3DP electron detector on the *Wind* spacecraft with 40–800 MHz solar observations by the AIP radio telescope in Potsdam-Tremsdorf, Germany. Other than preceding type III bursts, we find no single radio signature characteristic of the inferred electron injection times. The injection delays from the preceding type III bursts do not correlate with the 1 AU solar wind β_p or B_3 but do correlate with densities n_e and inversely with speeds V_{SW}, consistent with propagation effects. About half of the events are associated with metric or decametric-hectometric (dh) type II bursts, but most injections occur before or after those bursts. Electron events with long ($\geq$2 hr) beaming times at 1 AU are preferentially associated with type II bursts, which supports the possibility of a class of shock-accelerated NR electron events.

15. SUBJECT TERMS
Coronal mass ejections Particle emission Radio radiation

16. SECURITY CLASSIFICATION OF:			17. LIMITATION OF ABSTRACT	18. NUMBER OF PAGES	19a. NAME OF RESPONSIBLE PERSON
a. REPORT		c. THIS PAGE			S. W. Kahler
UNCLAS	UNCLAS	UNCLAS	SAR	10	19b. TELEPHONE NUMBER *(include area code)* 781-377-9665

THE ASTROPHYSICAL JOURNAL, 656:567–576, 2007 February 10

SOLAR RADIO BURST AND SOLAR WIND ASSOCIATIONS WITH INFERRED NEAR-RELATIVISTIC ELECTRON INJECTIONS

S. W. KAHLER
Air Force Research Laboratory, Space Vehicles Directorate, Hanscom AFB, MA

H. AURASS AND G. MANN
Astrophysikalisches Institut Potsdam, Potsdam, Germany

AND

A. KLASSEN
Institut für Experimentelle und Angewandte Physik, Universität Kiel, Kiel, Germany
Received 2006 February 2; accepted 2006 October 16

ABSTRACT

The solar injections of near-relativistic (NR) electron events observed at 1 AU appear to be systematically delayed by ~10 minutes from the associated flare impulsive phases. We compare inferred injection times of 80 electron events observed by the 3DP electron detector on the *Wind* spacecraft with 40–800 MHz solar observations by the AIP radio telescope in Potsdam-Tremsdorf, Germany. Other than preceding type III bursts, we find no single radio signature characteristic of the inferred electron injection times. The injection delays from the preceding type III bursts do not correlate with the 1 AU solar wind β_p or B, but do correlate with densities n_e and inversely with speeds V_{SW}, consistent with propagation effects. About half of the events are associated with metric or decametric-hectometric (dh) type II bursts, but most injections occur before or after those bursts. Electron events with long ($\geq$2 hr) beaming times at 1 AU are preferentially associated with type II bursts, which supports the possibility of a class of shock-accelerated NR electron events.

Subject headings: acceleration of particles — interplanetary medium — Sun: coronal mass ejections (CMEs) — Sun: particle emission — Sun: radio radiation

1. INTRODUCTION

The acceleration of near-relativistic (NR; $E > 30$ keV) electrons in the solar corona and their injection into space has been a subject of recent controversy. Early observations of 2–100 keV electron events at 1 AU suggested that impulsive acceleration occurs in solar flares accompanied by fast-drift metric and/or decametric type III radio bursts (Lin 1985) produced by beams of escaping electrons. However, recent results, based on observations of NR electron events by the Electron, Proton, and Alpha Monitor (EPAM) on the *Advanced Composition Explorer* (*ACE*) spacecraft (Haggerty & Roelof 2002; Haggerty et al. 2003) and by the 3-D Plasma and Energetic Particle (3DP) experiment on the *Wind* spacecraft (Krucker et al. 1999) at 1 AU, have indicated that in most events the solar injections are delayed from the type III burst times by up to half an hour.

Recent work has focused on comparisons of solar electron injection times with corresponding coronal EUV, white-light, and radio signatures to determine how the electron acceleration occurs. Krucker et al. (1999), Klassen et al. (2002), and Simnett et al. (2002) have argued for acceleration in coronal shocks. The inferred injections occur when the shocks, often producing type II radio bursts, or the coronal mass ejection (CME) shock drivers reach heights of ~1.5–4 $R_\odot$ from Sun center.

Kahler et al. (2005) looked for coronal shock associations of 100 $E \geq 25$ keV electron events (discussed in § 2) observed with the *Wind* 3DP instrument. Those electron events were compared with metric type II (hereafter type IIm) bursts observed by the radiospectrograph of the Astrophysikalisches Institut Potsdam (AIP), decametric-hectometric type II (hereafter type IIdh) bursts observed by the *Wind* WAVES instrument, and CMEs observed by the *Solar and Heliospheric Observatory* Large Angle Spectroscopic Coronagraph (*SOHO* LASCO) coronagraph. Only event associations were examined; the detailed relationships of the burst or CME times to inferred electron injection times were not considered. The associations of the electron events with type IIm (37%) and type IIdh (17%) bursts were not high, suggesting that most electron events do not originate in shocks. The 80% CME association was higher, but the consideration that shocks are driven only by wide (>60°) and fast (>900 km s^{-1}) CMEs (Gopalswamy et al. 2001) suggested an ~50% association of the electron events with fast and wide CMEs. Kahler et al. (2005) concluded that at least some, and perhaps most, NR electron events are not associated with coronal shocks.

Studies comparing inferred NR electron injections with metric radio coronal imaging observations from the Nançay Radioheliograph (NRH) have provided an alternative acceleration explanation for some events. Maia & Pick (2004) discussed 18 EPAM events (Haggerty & Roelof 2002), of which seven were consistent with injections during relatively simple radio signatures of type III bursts only. Injections of six of the 11 radio complex events occurred during NRH continuum emission consistent with acceleration and release of electrons during coronal magnetic reconnection, but not in CME-driven shocks. While shock acceleration could not be excluded in the five cases of radio complex events with type II bursts, Maia & Pick (2004) suggested shock-induced magnetic reconnection as the principal acceleration scenario.

A similar result was based on a survey of 40 3DP events (Klein et al. 2005), of which 10 showed no emission in the NRH frequency range of 164–432 MHz. In 18 of 30 cases with observed emission the inferred injection windows were in or close to a short

group of bursts, and in 12 of those 18 cases they were consistent with no delays from the first radio signatures of energetic electrons. In the 12 cases of injections during long (>10 minutes) periods of observed metric radio emission the relationships between injection and radio emission were complex, but the injections were always associated with new increases in radio emission. Although type II bursts were associated with at least 15 of the 30 NRH radio events and CMEs with 19 of the 26 NRH events with LASCO observations, Klein et al. (2005) argued that in most such cases the delayed electron injections were better matched to accelerations of radio-emitting electrons at heights lower than those of the shocks. They favored posteruptive magnetic reconnection as the sources of the NR electrons, similar to the conclusions of Maia & Pick (2004). In the same sense, without the need for traveling shock accelerators, Aurass et al. (2006) found evidence for several spatially distributed coronal magnetic field-related acceleration sites in analyzing the high-energy particle acceleration and escape for the X-class flare of 2003 October 28.

All the NR electron events observed at 1 AU are associated with dh type III bursts (Haggerty & Roelof 2002), which, at least for the events with delayed injections, are presumed to have no direct relevance to those electron events. A very different interpretation was suggested by Cane (2003), who found that the inferred injection delay times of 61 of the 79 Haggerty & Roelof (2002) EPAM electron events were correlated with the times for the radio-generating electrons to transit to 1 AU. In addition, a correlation of the delays was also found with the 1 AU ambient solar wind densities, leading her to conclude that interaction effects in the interplanetary medium were the cause of the inferred anomalous delays of the electron event onsets. This implies that the basic assumption that the first-arriving NR electrons propagate scatter-free, used to infer the electron solar injection times, is not valid. In this case there is only a single population of energetic electrons producing both the type III radio bursts and the events at 1 AU.

In this work we compare in detail a set of 80 3DP NR ($E >$ 25 keV) electron events with metric radiospectrographic observations of the AIP Tremsdorf Observatory and with solar wind parameters. These events are a subset of the 100 events used by Kahler et al. (2005) in their study of the possible shock origins of the NR electron events. After confirming the inferred injection delays from type III burst times, we examine in detail some of the properties of the electron events, their associated metric and decimetric radio bursts, and associated solar wind parameters. Our goal here is to use all the events of a large statistical data sample to understand the solar origins of the NR electron events. We look for correlations of the electron injection times with solar radio bursts and compare the injection delays with solar radio and solar wind characteristics.

2. DATA ANALYSIS

2.1. *Selection of the NR 3DP Electron Events*

The selection of the 3DP NR electron events for analysis was based on two previous event listings: (1) the electron events from the *Wind* 3DP solid-state telescope (SST) ranked as "mediocre" and "good" (S. Krucker 2003, private communication) and (2) the beamed events observed in the highest energy channels of the *ACE* EPAM instrument, given in Table 2 of Haggerty & Roelof (2002) and extended through the end of 2001 (D. Haggerty 2003, private communication). AIP Tremsdorf radio observations from about 1 hr before each inferred electron injection time through that injection time and *Wind* WAVES 20 kHz–14 MHz observations (Bougeret et al. 1995) through the event durations were required. Kahler et al. (2005) discussed the detailed selection criteria for the 100 events, of which we here use the subset of 80 events given in Table 1.

Along with Krucker et al. (1999) and Haggerty & Roelof (2002) we assume that the first observed electrons of each event have propagated scatter-free to 1 AU following a simultaneous solar injection at all electron energies. The event onset times were estimated by eye from the intensity time profiles of the 3DP SST. Solar injection times were derived from the apparent onset times of the 3DP 66–135 keV channel, using an effective electron energy E and $v_e/c = \beta$ of 82 keV and 0.507, respectively, with magnetic field path lengths calculated from the ambient solar wind speeds at times of onsets. The net result is that we subtracted 9–13 minutes from the 82 keV electron onset times at 1 AU to get the injection times relative to the observed solar radio times; the injection times are given in column (2) of Table 1. All events of the study showed strong pitch-angle anisotropy and velocity dispersion in their onsets. We did not attempt to do $1/\beta$ (Krucker et al. 1999) fits to derive the electron injection times. We find that the injection times of 14 of the 16 events of Table 1 in common with the 30 3DP events of the Klein et al. (2005) study lie within their ~6–10 minute injection time intervals, indicating good agreement with their injection determinations. In addition, our injection times differ by an average of only 2 minutes from those of the 13 EPAM electron events in common with the study of Maia & Pick (2004). Thus, the determination of the electron injection times by different techniques appears to give consistent results (Haggerty & Roelof 2002).

2.2. *The Injection Delay Times ΔT*

We generated high time resolution plots of WAVES radio emission in the 3.5 kHz–10 MHz range for the periods around the electron injection times. An associated *Wind* WAVES type IIIdh burst was found for all the electron events of Table 1 except that of 2000 March 6, for which there is a WAVES data gap. Figures 1–4 show examples of 0.02–14 MHz WAVES radio spectrograms combined with background-subtracted 40–800 MHz AIP spectrograms and the 3DP SST NR electron profiles with vertical dashed lines showing the solar electron injection times. For each type IIIdh burst we looked for a corresponding type IIIm burst in the AIP spectrograms and give in column (3) of Table 1 the onset times and qualitative assessments of the relative intensities (strong, moderate, or weak) of the most intense component of each type IIIm burst. Examples of strong bursts are shown in Figures 2 and 3. The first event of Figure 4 shows one of the 17 cases with no type IIIm burst preceding the electron injection by up to ~30–40 minutes. The second event of Figure 4 shows a barely visible weak type IIIm burst at 1131 UT. The highest MHz frequency at which the type IIIdh burst could be observed in the WAVES plots, $F_{\max}$, and the start and end times of the burst at $F_{\max}$ are given in columns (5) and (4), respectively, of Table 1. The two cases of low (~0.5 MHz) $F_{\max}$ in Figure 4 contrast sharply with those of high (10 MHz) $F_{\max}$ in Figures 1, 2, and 3.

The delay times, ΔT_m, between the inferred solar electron injections and the 63 associated type IIIm burst start times ranged from −2 to 53 minutes, with a median of 12 minutes. Figures 1, 2, and 4 show examples of short ($\leq$4 minutes) ΔT_m, and the event of Figure 3 is characterized by a long 21 minute ΔT_m. We expect the event delay times, $\Delta T_{\rm dh}$, relative to the type IIIdh bursts to be frequency dependent, decreasing with lower $F_{\max}$ as the dh emission drifts to lower frequencies at later times. Selecting only the 57 WAVES type IIIdh bursts with $F_{\max} \geq 3$ MHz, we find similar $\Delta T_{\rm dh}$ of −1 to 55 minutes and a median of

TABLE 1

SOLAR NR ELECTRON EVENTS AND ASSOCIATED FLARE RADIO AND SOLAR WIND OBSERVATIONS

Date (1)	Electron Injec. UT (2)	Metric III UT/int.[a] (3)	WAVES III UT (4)	WAVES F_{max} (5)	Type II Injection[b] (6)	PAD Dur.[c] (7)	S/N (8)	Decim Emis.[d] (9)	V_{SW} (km s^{-1}) (10)	log β_p (11)	Flare Site (12) (deg)
					1995						
Mar 6	0847	0826/md	0821–0830	10	A m/N dh	4	4.67	N	442	−0.9	S15, W58
Apr 2	0843	None	0830–0835	1	N II	0.2	1.33	N	360	−0.41	S13, W54
Apr 2	1112	1107/wk	1106–1108	10	N II	0.4	56.2	N	365	−0.45	S15, W54
Apr 2	1432	1423/wk	1420–1423	3	N II	0.3	8.3	IIIpc	352	−0.48	S15, W58
Oct 19	1122	1029/wk	1027–1030	10	N II	1.6	5.3	Y	415	−2.15	S14, W45
					1996						
Jul 1	1305	1234/md	1249–1257	0.8	A m/N dh	2	7	IIIpc	340	−0.18	N08, W83
Jul 9	0802	0751/wk	0753–0758	3	N II	1.4	3.71	Y	425	NA	S11, W23
Jul 9	0924	0912/stg	0910–0914	4	A m/N dh	1.5	53.8	Y	420	NA	S11, W30
Jul 14	1505	1446/stg	1445–1449	10	N II	0.3	9	IIIpc	378	NA	S10, W90
Aug 13	1551	None	1510–1516	1	A m/N dh	NA	7.5	N	370	−0.05	...
Dec 24	1316[e]	1306/wk	1305–1310	10	D m/N dh	1.2	50	IIIpc	373	−0.8	N05, W93
					1997						
Apr 7	1419	1401/stg	1356–1410	10	A m/B dh	1	100	Y	405	−0.15	S29, E20
May 12	0517	0457/md	0458–0503	10	A m/D dh	1	90	Y	305	−0.05	N21, W08
May 27	1026	0956/wk	0954–0958	10	N II	0.5	142.9	IIIpc	320	−0.88	N02, W76
Oct 7	1326	None	1251–1256	1	A m/N dh	6	50	N	335	0.21	SWL
Nov 6	1224[e]	1154/stg	1153–1157	10	A m/D dh	3.5	25	Y	350	0.24	S18, W63
Dec 18	1229	None	1203–1207	2	N II	1.5	5	IIIpc	300	−0.39	N19, E08
					1998						
Apr 20	1029[e,f]	1007/wk	1008–1030	1	A m/D dh	6	438	Y	370	−0.36	S43, W90
May 2	0500	0455/stg	0455–0508	10	N II	2	5.6	III	630	−1.2	S20, W10
May 2	1345[e]	1337/stg	1338–1344	10	D m/B dh	5	5.4	Y	600	−1.68	S15, W15
May 6	0801	0803/stg	0802–0807	10	B m/B dh	3	60	IIIpc	465	−2.02	S15, W64
May 27	1325[e]	1320/stg	1315–1325	10	N m/B dh	0.5	116.7	Y	470	0.1	N18, W60
Jun 15	0639	None	0610–0630	0.3	N II	0.5	1.4	Y	380	−0.58	S25, W90
Jun 16	1901[f]	(1822)/md	1826–1842	1	A m/D dh	NA	1.6	NA	400	−1.08	S20, W90
Jun 22	0452	None	0433–0443	2	A m/N dh	1.5	3	N	400	NA	N15, W46
Aug 13	1513	1508/stg	1505–1508	10	N II	3	2.3	IIIpc	360	−1.61	...
Aug 14	0606	0557/md	0556–0600	10	N II	0.5	5.4	IIIpc	385	−0.37	S23, W73
Sep 6	0612	0558/wk	0551–0557	2	N II	0.5	2.1	Y	355	−0.02	N30, W90
Sep 8	1528	1522/stg	1521–1525	10	N II	0.3	8	N	350	−1.57	...
Sep 27	0816[e]	0809/stg	0805–0812	10	N II	0.3	42.9	III	540	−0.18	N21, W48
Sep 30	1343[e,g]	None	1325–1333	10	A m/D dh	3	23.1	Y	420	−0.45	N20, W84
Nov 5	1347	1335/stg	1332–1340	10	N II	0.3	2.8	IIIpc	410	0.05	N15, W17

TABLE 1—*Continued*

Date (1)	Electron Injec. UT (2)	Metric III UT/int.[a] (3)	WAVES III UT (4)	WAVES F_{max} (5)	Type II Injection[b] (6)	PAD Dur.[c] (7)	S/N (8)	Decim Emis.[d] (9)	V_{SW} (km s^{-1}) (10)	log β_p (11)	Flare Site (12) (deg)
					1999						
Jan 24	1125	None	1112–1130	0.6	N II	0.2	2.1	N	525	0.18	N21, W30
Feb 20	1516	~1513/stg	1511–1518	10	N II	0.3	42.5	N	425	−1.8	S17, W71
Feb 21	0951	0943/stg	0945–0949	10	B m/N dh	NA	80	III	380	−1.18	...
Apr 24	1330	1312/wk	1300–1322	1	N m/B dh	0.2	15	Y	430	0.16	NWL
May 8	1442[e,g]	1425/stg	1424–1427	10	B m/N dh	NA	2.7	Y	415	−0.74	N23, W75
May 12	0658	0654/md	0654–0657	10	N II	0.2	4.4	IIIpc	470	−1.52	...
May 27	1057[e,g]	(1052)/md	1051–1056	10	A m/D dh	1.2	76.9	IIIpc	455	−0.44	WL
May 31	0956[e,g]	0937/stg	0935–0940	10	A m/N dh	2	4.5	IIIpc	360	−0.94	N18, W27
Jun 13	0526	0517/wk	0515–0518	10	N II	1.5	2.5	N	375	−0.48	...
Jun 18	0728	0711/md	0712–0715	3	N II	I	4.9	III	390	−0.36	...
Jun 18	1143	1129/md	1129–1132	10	N II	I	8	III	380	−0.22	...
Jun 18	1438	1424/md	1423–1427	10	N II	I	8	IIIpc	380	−0.23	...
Jun 18	1657	1641/stg	1638–1644	10	A m/N dh	I	3.3	IIIpc	375	−0.15	...
Jun 23	0605	0544/wk	0541–0545	10	A m/D dh	2	7.9	IIIpc	310	−0.53	...
Jul 16	1604	1552/wk	1552–1556	10	D m/N dh	0.5	20	IIIpc	350	−0.21	NWL
Jul 20	0841	0819/md	0818–0821	6	N II	NA	2.5	IIIpc	290	−0.07	S12, W70
Oct 27	0924	0910/stg	0908–0915	10	D m/N dh	I	8.8	IIIpc	395	−0.36	S12, W15
					2000						
Feb 18	0927[e,f,g,h]	None	0925–0928	2	D m/N dh	2.5	33.3	NA	400	−0.86	NWL
Mar 2	0838[g]	0825/stg	0824–0829	10	A m/N dh	1.7	10	NA	435	−0.51	S14, W52
Mar 6	1221[e]	1211/md	Data Gap	DG	N II	1.5	3.3	IIIpc	435	−0.45	...
Mar 7	0736	0724/md	0724–0727	10	N II	I	10	NA	440	−0.6	...
Mar 7	1237	1229/wk	1229–1233	10	N II	0.7	23.3	NA	440	−0.64	S11, W14
Mar 7	1518[e]	1512/wk	1512–1516	10	N II	0.3	2.9	NA	435	−0.61	...
Mar 19	1304	1245/wk	1244–1248	10	N II	NA	16.7	NA	355	1.29	...
Apr 4	1520[g]	1518/stg	1517–1522	10	B m/N dh	0.8	350	Y	380	−0.4	N16, W66
Apr 19	1238[e]	1231/stg	1229–1233	10	N II	1.5	2	IIIpc	430	−0.49	...
Apr 27	1425	None	1416–1423	1	N II	0.7	3.8	N	410	−0.3	N32, W90
					2001						
Apr 30	1057[e]	1058/wk	1057–1059	10	N II	0.4	11.4	IIIpc	440	−1.82	N30, WL
					2002						
Feb 20	1114	1106/stg	1104–1109	10	N II	1	2.5	IIIpc	390	−0.72	N15, W77
Feb 25	1217	1205/wk	1204–1206	10	N II	0.2	3	N	360	NA	S01, W51
Feb 27	1211	1158/md	1157–1200	5	N II	1	3	IIIpc	345	−0.62	N23, W15
Mar 22	1109	1049/wk	1049–1051	10	D m/B dh	1.2	5	N	440	−0.22	S10, WL
Mar 27	1457	1441/wk	1439–1444	5	N II	0.3	11.8	N	480	−0.22	...
Mar 28	0839	0823/wk	0821–0824	5	N II	0.5	12	N	380	−0.2	S25, WL
Apr 11	1629	1618/wk	1618–1624	10	D m/N dh	3	66.7	IIIpc	468	−0.58	S15, W33
Apr 15	1752	(None)	1725–1735	1	N II	0.8	8.8	N	359	−0.4	S16, W60

TABLE 1—*Continued*

Date (1)	Electron Injec. UT (2)	Metric III UT/int.[a] (3)	WAVES III UT (4)	WAVES F_{max} (5)	Type II Injection[b] (6)	PAD Dur.[c] (7)	S/N (8)	Decim Emis.[d] (9)	V_{SW} (km s^{-1}) (10)	log β_p (11)	Flare Site (12) (deg)
					2002						
May 20	1546	1525/stg	1524–1533	10	A m/N dh	0.4	3	IIIpc	446	−1.05	S21, E65
May 30	0522	0518/wk	0457–0509	0.5	N II	2.5	17.5	Y	514	−0.03	N10, WL
Jun 2	1026[i]	(None)	1014–1017	10	D m/N dh	0.4	11.1	Y	399	−0.03	S20, W61
Jun 30	0922	None	0900–0910	1	N II	0.7	2.7	Y	367	−0.2	...
Jul 7	1149	1115/md	1117–1125	1	N m/D dh	7	20	IIIpc	423	−0.45	...
Aug 3	1335	(None)	1324–1327	10	N II	0.4	1.9	N	442	−0.95	...
Aug 16	0609	(None)	0557–0601	4	N m/B dh	1.1	59.1	N	577	−0.2	N07, W83
Sep 24	1118	None	1115–1121	0.5	N II	1.4	12	N	366	NA	S05, WL
Sep 24	1133	1131/wk	1132–1142	0.5	N II	1.4	13.3	N	366	NA	S05, WL
Sep 26	1234	None	1221–1230	1	N II	0.4	4	N	345	NA	...
Oct 20	1145	1135/wk	1136–1140	1	N II	0.2	2.5	N	664	−0.63	N25, E55
Oct 20	1418	1412/md	1411–1414	5	B m/N dh	0.8	50	N	649	−0.52	S13, W63

[a] Metric type III burst UT onset times and relative intensities (stg = strong; md = moderate; wk = weak).
[b] Electron injection times relative to AIP metric (m) or WAVES decametric-hectometric (dh) type II bursts, if any (A = after; B = before; D = during; N II = no type II burst).
[c] Time in hours during which the PAD plots showed clear beaming.
[d] Observed decimetric (>200 MHz) emission. N = none; Y = new emission preceding electron injection; III = extension of type III burst only; IIIpc = associated preceding type III burst only; N = data gap.
[e] Described in Klein et al. (2005).
[f] Described in Klassen et al. (2002).
[g] Described in Maia & Pick (2004).
[h] Described in Haggerty & Roelof (2002) and Simnett et al. (2002).
[i] Described in Classen et al. (2003).

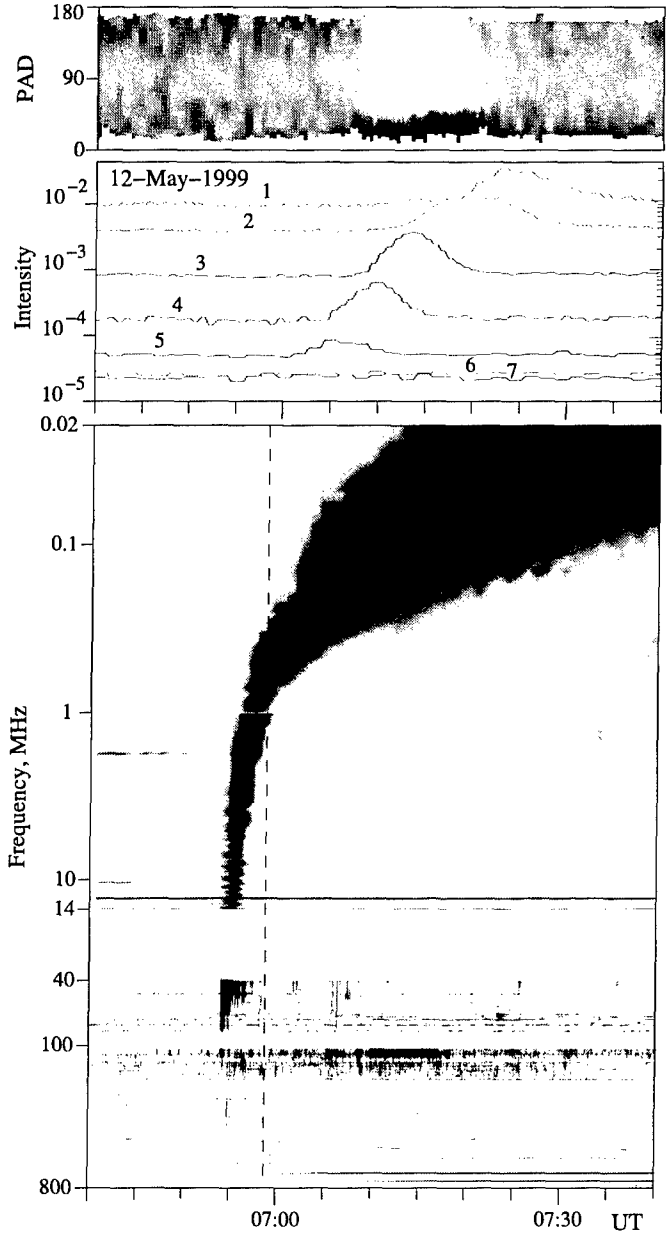

FIG. 1.—Electron event of 1999 May 12. *Top*: Normalized PAD of the 3DP channel 3, corresponding to an average energy of ~82 keV. *Middle*: Counting rate profiles of 3DP SST channels 1–7 covering the energy range ~25 to ~500 keV. *Bottom*: Composite profile of radio emission from 20 kHz to 14 MHz (*Wind* WAVES) and 40–800 MHz (AIP Tremsdorf). The vertical dashed line indicates the inferred solar electron injection time based on the onset time of the channel 3 counting rates of ~82 keV electrons; the injection time is advanced 500 s to match the radio emission profile. This electron event had no associated type II burst, a short ~0.2 hr PAD beaming time, and a short 4 minute injection delay time.

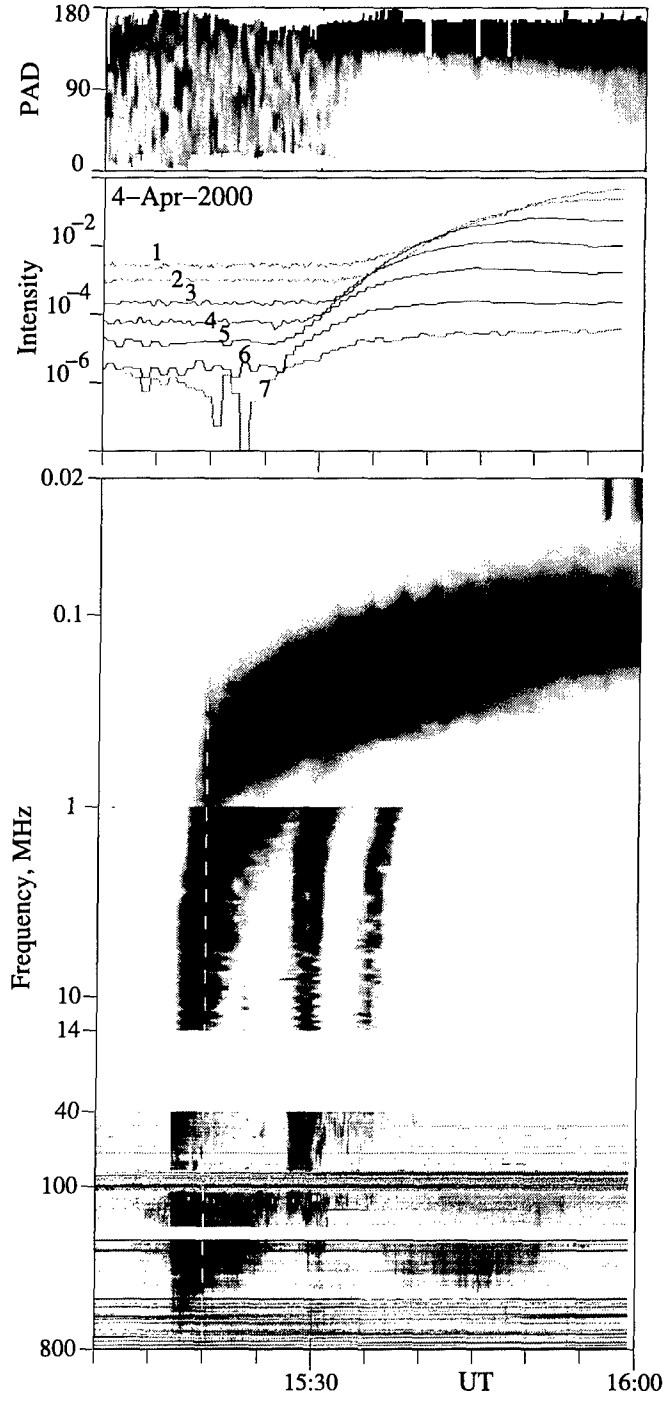

FIG. 2.—Electron event of 2000 April 4. The panel formats are the same as in Fig. 1. The inferred solar injection occurred before the 1524.8 UT onset of a short type IIm burst but during a time of significant decimetric emission. The electron injection delay of 2 minutes is one of the shortest of the 80 events of the study.

12 minutes. We also ask whether ΔT_m or ΔT_{dh} depends on the intensities of the electron events, such that onsets of more intense electron events are observed earlier due to their higher signal-to-noise ratios (S/Ns) in the 3DP detector. S/Ns of the 3DP 82-keV electron channel background-subtracted peak counting rates to the pre-event background rates are given in column (8) of Table 1. No correlation between the delay times and their S/Ns was found.

We looked for flare associations for all the events of Table 1 and were able to make associations for the 59 events shown in column (12). The locations were determined on the basis of Hα flare reports and X-ray and EUV images from the *Yohkoh* SXT and *SOHO* EIT instruments, respectively. We could not determine possible flare locations for the remaining 21 events. The flare locations are generally magnetically well connected to the Earth. Eleven are at or over the west limb (WL). Of the four flares located in the eastern hemisphere, two (1997 December 18 and 2002 October 20) are not associated with *GOES* X-ray flares and may not be true associations. We used the solar wind speeds of column (10) to calculate the longitudinal angular displacements of the Earth magnetic footpoints from the solar flare sites, setting the WL longitudes to be W100°. We found no dependence on flare longitudinal separation for either ΔT_m (46 cases) or ΔT_{dh} with $F_{max} \geq 3$ MHz (41 cases).

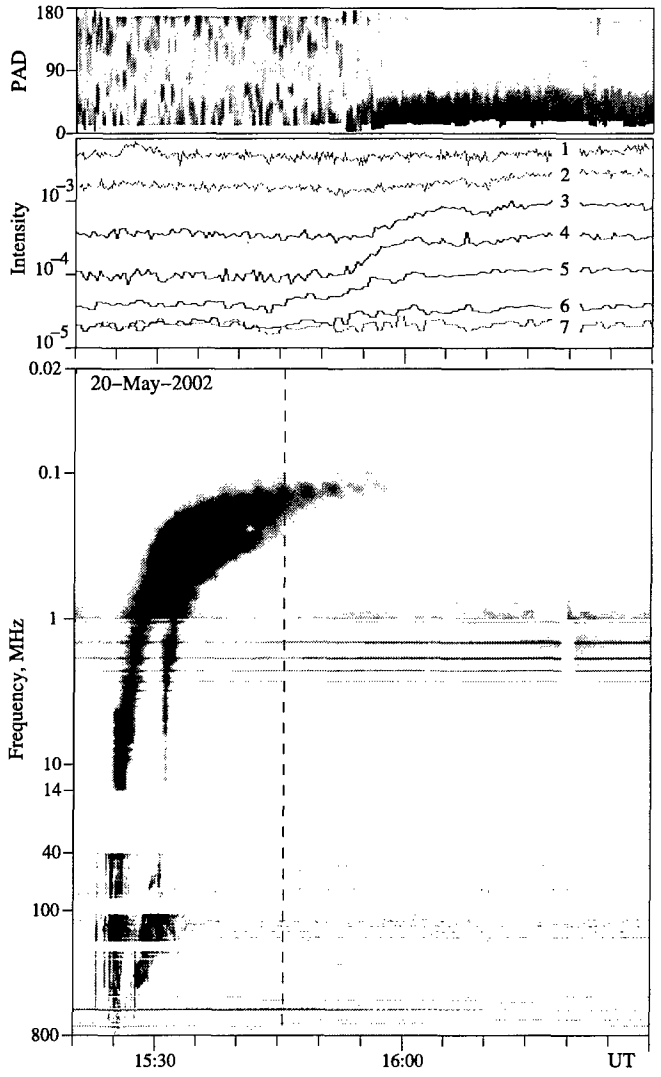

FIG. 3.—Electron event of 2002 May 20. The panel formats are the same as in Fig. 1. The inferred electron injection occurred well after the type IIm burst, which ended at 1532 UT. This event has a long (≥17 minutes) electron injection delay and is one of four associated with an eastern hemisphere flare.

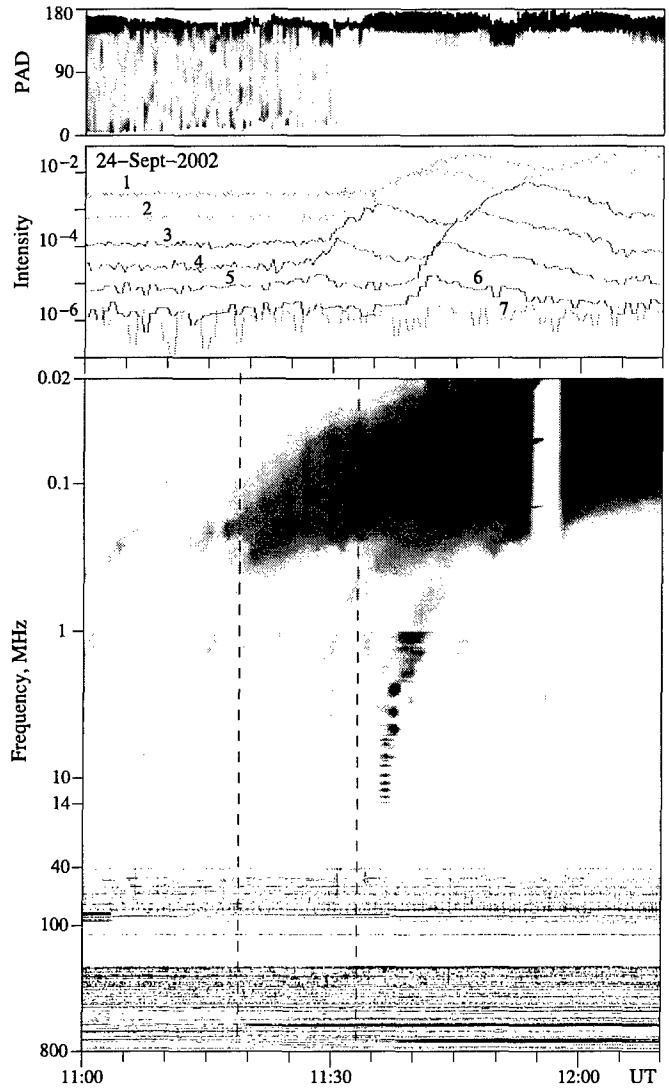

FIG. 4.—Two electron events of 2002 September 24. The panel formats are the same as in Fig. 1. The type IIIm burst was weak in the second event and absent in the first. There was no type II or decimetric emission associated with either injection.

2.3. *Event Comparisons with Type III, Type II, and Decimetric Bursts*

We divide the 63 NR electron events of Table 1 with associated type IIIm bursts into three approximately equal groups of 21 short (≤8 minutes), 22 intermediate (9–16 minutes), and 20 long (≥17 minutes) ΔT_m. In Figure 5 we compare those three groups with various radio parameters to see whether ΔT_m organizes any of those parameters. The top panel shows associations of the three groups with the type IIIm burst intensities of the third column of Table 1. There is only a slight tendency for the short-delay group to be associated with strong type IIIm bursts; otherwise, ΔT_m shows no dependence on the type IIIm burst intensities.

There were 31 and 15 NR electron events associated with type IIm and type IIdh bursts, respectively, and their injection times relative to the type II burst durations (before, during, or after) are shown in column (6) of Table 1. The type IIm burst start and end times were taken from the AIP plots and those of type IIdh from the WAVES list.[1] We find that only eight of the 80 NR electron injections occurred during type IIm bursts and a different set of eight during type IIdh bursts. Because of the frequency gap of ~25 MHz between the Tremsdorf and WAVES receivers, the injection on 1997 April 7 after the type IIm and before the type IIdh burst (listed in Table 1 as "A m/B dh") can also be a case of injection while the shock was crossing the frequency gap. Thus, injections occurred during type II bursts in at most 17 of the 80 NR electron events. The middle panel of Figure 5 shows the distributions by groups of ΔT_m for the 25 and 13 NR electron injections associated with type IIm and type IIdh bursts. As we should expect, the injections with short (long) ΔT_m are more likely to occur before (after) the times of the type II bursts.

Decimetric emission at $f > 200$ MHz was examined in the AIP radiospectrograms to look for evidence of energetic electron production in the lower corona. If decimetric emission was present within ±2 minutes of the inferred injection time, we give the burst classification in column (9) of Table 1 as the high-frequency component of a type IIIm burst (III) or as a burst of new emission (Y), probably an extension of a microwave or metric type IV burst. Otherwise, there was no emission (N), a data gap (NA), or only an earlier $f > 200$ MHz component of the associated preceding metric type III burst (IIIpc). The associations

[1] See http://lep694.gsfc.nasa.gov/waves/waves.html.

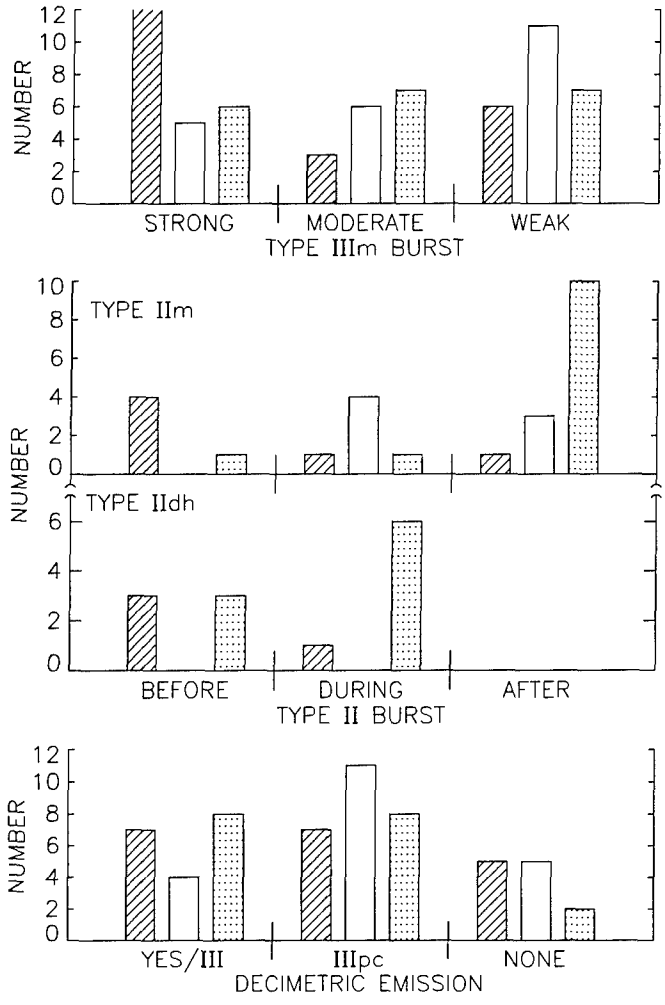

FIG. 5.—Distributions of numbers of the 63 NR electron events with different ΔT_m for various associated radio burst parameters. Striped, open, and stippled bars are short (<8 minutes), intermediate (9–16 minutes), and long (≥17 minutes) ΔT_m, respectively. *Top*: Associations with strong, moderate, and weak type IIIm bursts. *Middle*: Associations with NR electron injections before, during, or after the observed times of type IIm (upper) or type IIdh (lower) bursts. *Bottom*: Associations with NR electron injections during $f > 200$ MHz decimetric bursts (Y/III), only following preceding type III bursts (IIIpc), or with no bursts (NONE).

are given in the bottom panel of Figure 5 for the three groups of different ΔT_m. Only 23 (18 Y and 5 III) of the 73 events with available observations are associated with simultaneous decimetric emission. The distribution of the ΔT_m groups in the Y/III association is not significantly different from those of the IIIpc and N categories.

2.4. *Delay Time Comparisons with Ambient Solar Wind Parameters*

Following the work of Cane (2003), we compare ΔT_m with ambient solar wind parameters measured at 1 AU. In columns (10) and (11) of Table 1 we list the solar wind speeds V_{SW} and the logs of the plasma β_p values computed from *Wind* measurements of n_e and B. Neither ΔT_m nor ΔT_{dh} is significantly correlated with the logs of β_p or with B. Both ΔT_m and ΔT_{dh} are weakly negatively correlated with V_{SW} at $r = 0.31$ and 0.33, respectively, and a 99% confidence level (Fig. 6). Furthermore, by deleting one outlier event with very high values of ΔT (1995 October 19) and another with a very high n_e (2000 March 19), we find correlations of $r = 0.38$ and 0.40 (99% confidence levels) for ΔT_m

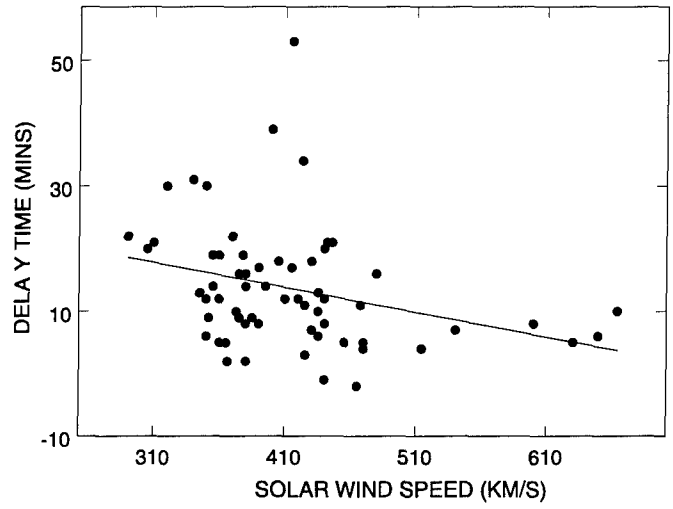

FIG. 6.—Correlation of ΔT_m vs. the V_{SW} measured at *Wind*. The line shows the least-squares best fit to the 63 points. The correlation coefficient $r = 0.31$.

and ΔT_{dh}, respectively, with n_e. Finally, a negative correlation of $r = 0.40$ (99% confidence level) exists between V_{SW} and n_e.

2.5. *Anisotropic PAD Durations*

Another NR electron event parameter, given in column (7) of Table 1, is the approximate time over which the event pitch-angle distribution (PAD) remained highly anisotropic, indicating a clear antisunward beaming of electrons. These times, based on qualitative assessments of color-coded PADs of the 82 keV electrons, ranged from 0.2 to 7 hr. The top panels of Figures 1 and 3 illustrate gray-scale PADs with beaming durations of less than the 1 hr median value; the 1.4 hr duration of the two events of Figure 4 is relatively long. In six cases, indicated as NA, the 3DP plot did not include enough of the PAD at 0° and 180° to make a good determination of the beaming time. Neither ΔT_m nor ΔT_{dh} are correlated with the PAD beaming durations.

We find no significant correlations of the beaming durations with any of the solar wind parameters V_{SW}, β_p, B, or n_e, suggesting that the extended electron beaming times reflect the durations of the injections rather than the particle transport properties. This may mean two kinds of solar injection, perhaps one impulsive at well connected flare sites and the other extended at broad CME-driven shocks. Supporting this possibility is the result that the 16 NR electron events with the longest (≥2 hr) PAD beaming durations are well associated with the presence of m/dh type II bursts, in contrast to the 14 with the shortest (≤0.3 hr) durations, as indicated in Table 2.

We can use longitudinal angular displacements of the Earth magnetic footpoints from the solar flare sites (Table 1) as a further test of the idea of two kinds of solar injection. The median

TABLE 2
NR ELECTRON PAD BEAMING DURATIONS AND TYPE II BURST ASSOCIATIONS

TYPE II BURST DESCRIPTOR	BEAM DURATION		
	Short[a]	Intermediate[b]	Long[c]
m/dh Type II	1	17	13
No Type II	13	27	3

[a] Beam durations ≤0.3 hr.
[b] Beam durations 0.4–1.7 hr.
[c] Beam durations ≥2 hr.

flare longitudinal displacement of the 13 long-duration PAD beamed events associated with flare sites is 26°, somewhat wider than the 15° of the 10 short-duration beamed events. However, comparing more broadly the flare locations of the No type II events of Table 1, assumed to be impulsive flare injections, with those of the m/dh type II bursts, assumed to be shock injections, we find comparable median flare displacements of 26° for the 29 No type II events and 29° for the 30 m/dh type II events. Thus, while the flare longitude displacements provide some support for impulsive flare and extended shock injection for the shortest and longest injections, respectively, such a distinction between the two kinds of suggested electron injections for all events is not obvious based on these simple event associations with type II bursts.

3. DISCUSSION

3.1. *Interpretation of the Injection Delay Times*

We have selected 80 3DP NR electron events for a statistical study to determine the solar conditions of their injections. In each case we determined an onset of the solar injection time based on the 82 keV electron onset at the 3DP and the assumption of scatter-free interplanetary propagation. Similar event surveys (e.g., Klein et al. 2005; Maia & Pick 2004) have further selected for detailed comparison only those events with significant associated solar radio bursts during the injection times. Complex or long-duration ($\geq$10 minutes) metric radio bursts were associated with 11 of the 21 electron events of Maia & Pick (2004) and 12 of the 40 electron events of Klein et al. (2005). Remaining events had either short-duration emission, typically type III bursts, or no emission in the metric/decametric range. Thus, the interpretation of the solar acceleration and injection conditions has been focused on bursts that are not representative of all observed NR electron events. We have indicated in Table 1 which electron events have been included in other detailed studies; in particular, the 2000 February 18 event has been analyzed in the works of four different groups. Our goal here is to describe all 80 electron events statistically.

We confirm the values of ΔT found by others. Our median time for ΔT_m is 12 minutes, and the times range from -2 to 55 minutes, although only one event exceeded 39 minutes. The $\Delta T_{\rm dh}$ values are similar. The longitudinal footpoint displacements of Hα flare locations do not order ΔT, as Haggerty et al. (2003; their Fig. 1) found. Furthermore, ΔT depends on neither the peak intensities of the NR electron events themselves nor the intensities of the associated type IIIm bursts (Fig. 5).

We used the AIP and WAVES radiospectrograms to examine the associations of the NR electron injections with $f > 200$ MHz decimetric emission. The bottom panel of Figure 5 indicates that only 18 of 73 (25%) injection times occurred during emissions other than accompanying or preceding type III bursts. These 18 events may correspond to the group of long-duration or complex bursts selected for detailed study in the metric range by Klein et al. (2005) and Maia & Pick (2004). We do not find a significant difference between the short and long ΔT_m events in these associations. In general we find a lack of any consistent signature other than the presence of preceding type III bursts for the events of the study.

Cane (2003) favored a single population of energetic electrons producing both the preceding type III radio bursts and the NR electron events at 1 AU. Haggerty & Roelof (2002) used the type III burst drift rates between the 14 and 2 MHz peak intensities to argue that the burst exciter speeds were $\sim c/12$, corresponding to electrons of $\sim$2 keV that constitute a population separate from the NR population. However, Mann & Klassen (2005) made clear that the electron beams producing type III bursts evolve in space and time, so that different parts of the electron distributions are responsible for the type III burst radiation at different locations (i.e., frequencies) during their coronal propagation. Thus, contrary to the Haggerty & Roelof (2002) argument, NR electrons could be injected in type III bursts.

Cane (2003) also argued for an unspecified interaction effect in the interplanetary medium as the main cause of the delayed onsets. Evidence for that effect was that the ΔT correlate with n_p. In our events we also found correlations of ΔT_m ($r = 0.38$) and $\Delta T_{\rm dh}$ ($r = 0.40$) with n_p; our r values are slightly less than her $r = 0.41$. However, for interplanetary interactions we might also expect the ΔT to increase with the NR electron travel distance to 1 AU, hence to decrease with $V_{\rm SW}$, as we found (Fig. 6). Thus, because of the general inverse correlation between n_p and $V_{\rm SW}$ (Burlaga 1995 and our § 2.4) and the inverse correlation of ΔT and n_p, any NR electron onset delays due to a propagation effect are not necessarily due to enhanced n_p. We looked for further evidence that the electron injection delay times may be correlated with solar wind properties. Because of the general inverse correlation between in situ particle anisotropies and solar wind β_p (Crooker et al. 2003) we compared the injection delay times with β_p, as well as with B and n_p, and found no correlations with β_p or with B.

3.2. *Impulsive Phase and Shock Injections*

NR electron acceleration at CME-driven shocks is a strong possibility (Simnett et al. 2002; Kahler et al. 2005) when type II bursts are associated with the NR electron events. Only 31 and 15 of the 80 events of the study were associated with type IIm and type IIdh bursts, respectively, suggesting that shocks were not the sources of the majority of events. We also note that the presence of type II bursts may not be a good guide to shock acceleration of NR electrons, judging by the comparable longitudinal footpoint displacements for the flares of NR electron events with and without type II bursts. On the other hand, of the 20 NR electron events with long ($\geq$17 minutes) ΔT_m, 14 were associated with type II bursts, suggesting injections from shocks for most of those events, even though the inferred injections often occurred before or after the type II burst times (Fig. 5, *middle*).

We assume that NR electron shock acceleration and injection occurs over times significantly longer than those of impulsive injections. The estimated PAD beaming durations are not correlated with the solar wind β_p (Crooker et al. 2003) or other solar wind parameters and thus serve as guides to injection durations. We separated out two event groups of long- and short-duration PAD beaming durations to compare with type II bursts with the idea that electrons of the long-duration group are injected over longer times and larger spatial regions from shocks and that electrons of the short-duration group may be injected only over the short intervals of the type III bursts from well-connected source regions. The result in Table 2 that the long-duration group is much better associated with type II bursts supports this idea with, of course, limited statistics. The longitudinal footpoint displacements of the Hα flares of long-duration beamed events exceeded those of short-duration events by 26° versus 15°, consistent with a shock origin for the former events.

We take these results as weak support for two different kinds of injections. The first is impulsive, during or shortly delayed from type III bursts, characterized by smaller ΔT_m and shorter PAD beaming durations, and the second from shocks, characterized by larger ΔT_m and longer PAD beaming durations. However, further statistical support for this scheme is not forthcoming. Neither a possible expected bimodal distribution in ΔT_m

(Haggerty et al. 2003) nor a correlation between ΔT_m and PAD beaming durations (§ 2.5) has been found. These negative results could be due to effects such as both kinds of injections occurring in single NR electron events, variable delays between flare impulsive phases and shock injections, or from interplanetary scattering producing variable onset delays in both kinds of events. The observed distribution of ΔT_m could therefore result from a combination of delays due to interplanetary scattering and solar injections delayed from the flare impulsive phases.

We thank S. Krucker for his help and advice with access to the 3DP software, D. Haggerty for the EPAM event list, H. Cane for sharing her event flare associations, and the referee for helpful advice on the manuscript. S. K. thanks the AIP for their hospitality and the Air Force Office of Scientific Research for funding his Window on Europe visit to the AIP. The AIP acknowledges the European Office for Aerospace Research and Development for its support in maintaining the solar radio spectral observations at Potsdam.

REFERENCES

Aurass, H., Mann, G., Rausche, G., & Warmuth, A. 2006, A&A, 457, 681
Bougeret, J.-L., et al. 1995, Space Sci. Rev., 71, 231
Burlaga, L. F. 1995, Interplanetary Magnetohydrodynamics (New York: Oxford Univ. Press)
Cane, H. V. 2003, ApJ, 598, 1403
Classen, H. T., Mann, G., Klassen, A., & Aurass, H. 2003, A&A, 409, 309
Crooker, N. U., Larson, D. E., Kahler, S. W., Lamassa, S. M., & Spence, H. E. 2003, Geophys. Res. Lett., 30, 21, DOI: 10.1029/2003GL017036
Gopalswamy, N., Yashiro, S., Kaiser, M. L., Howard, R. A., & Bougeret, J.-L. 2001, J. Geophys. Res., 106, 29219
Haggerty, D. K., & Roelof, E. C. 2002, ApJ, 579, 841
Haggerty, D. K., Roelof, E. C., & Simnett, G. M. 2003, Adv. Space Res., 32, 2673
Kahler, S. W., Aurass, H., Mann, G., & Klassen, A. 2005, in IAU Symp. 226, Coronal and Stellar Mass Ejections, ed. K. P. Dere et al. (Cambridge: Cambridge Univ. Press), 338
Klassen, A., Bothmer, V., Mann, G., Reiner, M. J., Krucker, S., Vourlidas, A., & Kunow, H. 2002, A&A, 385, 1078
Klein, K.-L., Krucker, S., Trottet, G., & Hoang, S. 2005, A&A, 431, 1047
Krucker, S., Larson, D. E., Lin, R. P., & Thompson, B. J. 1999, ApJ, 519, 864
Lin, R. P. 1985, Sol. Phys., 100, 537
Maia, D. J., & Pick, M. 2004, ApJ, 609, 1082
Mann, G., & Klassen, A. 2005, A&A, 441, 319
Simnett, G. M., Roelof, E. C., & Haggerty, D. K. 2002, ApJ, 579, 854